Structural and Physical Properties of Heavily Doped Yttrium Vanadate: $Y_{0.6}Cd_{0.4}VO_3$

Alexei A. Belik,*,† Masahiro Nagao,‡ Masaki Azuma,§ Mikio Takano,§ Yoshio Matsui,‡ and Eiji Takayama-Muromachi†

International Center for Materials Nanoarchitectonics (MANA) and High Voltage Electron Microscopy Station (HVEMS), National Institute for Materials Science (NIMS), 1-1 Namiki, Tsukuba, Ibaraki 305-0044, Japan and Institute for Chemical Research, Kyoto University, Uji, Kyoto-fu 611-0011, Japan

Received April 2, 2008. Revised Manuscript Received June 3, 2008

Structural properties of $Y_{0.6}Cd_{0.4}VO_3$ were investigated by electron diffraction and laboratory and synchrotron X-ray powder diffraction methods. $Y_{0.6}Cd_{0.4}VO_3$ crystallizes in space group *Pnma* ($GdFeO_3$-type perovskite structure) between 12 and 300 K ($a = 5.45887(3)$ Å, $b = 7.57250(4)$ Å, and $c = 5.27643(2)$ Å at 300 K). The lattice parameters showed anomalous behavior on temperature. The *c* parameter linearly decreased from 12 to 120 K, and then it lineally increased from 160 to 300 K. The *b* parameter was constant between 12 and 120 K, demonstrated a drop from 120 to 200 K, and then lineally increased from 200 to 300 K. The *c*/*a* ratio had a rather sharp maximum at 150 K. In $Y_{0.6}Cd_{0.4}VO_3$ the V−O distances in the *ac* plane began to split to shorter and longer ones below 150 K, indicating that orbital fluctuations are involved. The phase transition near 150 K in $Y_{0.6}Cd_{0.4}VO_3$ is accompanied by a broad anomaly on the specific heat and change of the slope of the inverse magnetic susceptibility. Other members of the $Y_{1-x}Cd_xVO_3$ solid solution with $x = 0.3$, 1/3, and 0.5 did not show this kind of phase transition. This kind of a phase transition has never been detected in other doped vanadates, $R_{1-x}M_xVO_3$ (R = Y and rare earths and M = Ca and Sr).

1. Introduction

The magnetic properties of highly correlated d-electron systems are presently of great interest. One aspect of interest is the insulator−metal (IM) transition driven by carrier doping.[1,2] The prototypical systems of the doped IM transition are, for example, high T_c superconducting copper oxides. YVO_3 is a typical Mott−Hubbard antiferromagnetic insulator with V^{3+} ($S = 1$, S is spin) magnetic ions. Magnetic properties of YVO_3 have received a lot of attention in connection with different spin and orbital orders.[1–11] Two antiferromagnetic phase transitions occur at $T_N = 116$ K and $T_S = 77$ K, and two types of orbital ordering were observed below $T_O = 200$ K and T_S. YVO_3 crystallizes in the $GdFeO_3$-type perovksite structure (space group *Pnma*; lattice parameters $a = 5.6061$ Å, $b = 7.5742$ Å, and $c = 5.2784$ Å).[6,10] $CaVO_3$ has the same crystal structure (space group *Pnma*; $a = 5.3171$ Å, $b = 7.5418$Å, and $c = 5.3396$ Å).[12] Stoichiometric $CaVO_3$ is metallic; however, the electronic properties of $CaVO_3$ strongly depend on the oxygen content.[13,14]

Because YVO_3 and $CaVO_3$ are isostructural, solid solutions between them have attracted attention as another prototypical system of the doped IM transition.[1,2,8,13–19] In $Y_{1-x}Ca_xVO_3$, the nominal valence of V changes from +3 in YVO_3 to +4

* To whom correspondence should be addressed. E-mail: Alexei.BELIK@nims.go.jp.
† MANA, NIMS.
‡ HVEMS, NIMS.
§ Kyoto University.

(1) Ishihara, S. *Phys. Rev. Lett.* **2005**, *94*, 156408.
(2) (a) Fujioka, J.; Miyasaka, S.; Tokura, Y. *Phys. Rev. B* **2005**, *72*, 024460. (b) Fujioka, J.; Miyasaka, S.; Tokura, Y. *Phys. Rev. B* **2008**, *77*, 144402.
(3) (a) Nguyen, H. C.; Goodenough, J. B. *Phys. Rev. B* **1995**, *52*, 324. (b) Zhou, J.-S.; Goodenough, J. B.; Yan, J.-Q.; Ren, Y. *Phys. Rev. Lett.* **2007**, *99*, 156401.
(4) (a) Ren, Y.; Palstra, T. T. M.; Khomskii, D. I.; Nugroho, A. A.; Menovsky, A. A.; Sawatzky, G. A. *Phys. Rev. B* **2000**, *62*, 6577. (b) Ren, Y.; Palstra, T. T. M.; Khomskii, D. I.; Pellegrin, E.; Nugroho, A. A.; Menovsky, A. A.; Sawatzky, G. A. *Nature* **1998**, *396*, 441.
(5) Blake, G. R.; Palstra, T. T. M.; Ren, Y.; Nugroho, A. A.; Menovsky, A. A. *Phys. Rev. Lett.* **2001**, *87*, 245501.
(6) Blake, G. R.; Palstra, T. T. M.; Ren, Y.; Nugroho, A. A.; Menovsky, A. A. *Phys. Rev. B* **2002**, *65*, 174112.
(7) (a) Ulrich, C.; Khaliullin, G.; Sirker, J.; Reehuis, M.; Ohl, M.; Miyasaka, S.; Tokura, Y.; Keimer, B. *Phys. Rev. Lett.* **2003**, *91*, 257202. (b) Horsch, P.; Khaliullin, G.; Oles, A. M. *Phys. Rev. Lett.* **2003**, *91*, 257203.
(8) Sage, M. H.; Blake, G. R.; Palstra, T. T. M. *Phys. Rev. B* **2008**, *77*, 155121.
(9) Fang, Z.; Nagaosa, N. *Phys. Rev. Lett.* **2004**, *93*, 176404.
(10) Reehuis, M.; Ulrich, C.; Pattison, P.; Ouladdiaf, B.; Rheinstadter, M. C.; Ohl, M.; Regnault, L. P.; Miyasaka, M.; Tokura, Y.; Keimer, B. *Phys. Rev. B* **2006**, *73*, 094440.
(11) Solovyev, I. V. *Phys. Rev. B* **2006**, *74*, 054412.
(12) Garcia-Jaca, J.; Mesa, J. L.; Insausti, M.; Larramendi, J. I. R.; Arriortua, M. I.; Rojo, T. *Mater. Res. Bull.* **1999**, *34*, 289.
(13) (a) Zhou, H. D.; Goodenough, J. B. *Phys. Rev. B* **2004**, *69*, 245118. (b) Falcón, H.; Alonso, J. A.; Casais, M. T.; Martínez-Lope, M. J.; Sánchez-Benítez, J. *J. Solid State Chem.* **2004**, *177*, 3099, and references therein.
(14) Pen, H. F.; Abbate, M.; Fuijmori, A.; Tokura, Y.; Eisaki, H.; Uchida, S.; Sawatzky, G. A. *Phys. Rev. B* **1999**, *59*, 7422, and references therein.
(15) Kasuya, M.; Tokura, Y.; Arima, T.; Eisaki, H.; Uchida, S. *Phys. Rev. B* **1993**, *47*, 6197.
(16) Cintolesi, F.; Corti, M.; Rigamonti, A.; Rossetti, G.; Ghigna, P.; Lascialfari, A. *J. Appl. Phys.* **1996**, *79*, 6624.
(17) Cintolesi, F.; Ghigna, P.; Lascialfari, A.; Parravicini, G. B. *Phys. Chem. Chem. Phys.* **2003**, *5*, 4691.
(18) Nakotte, H.; Alsmadi, A. M.; Kawanaka, H.; Kindo, K.; Goto, K. *Int. J. Modern Phys. B* **2002**, *16*, 3058.
(19) Kumagai, K.; Kawano, K.; Suzuki, T.; Takahashi, H.; Kasuya, M.; Fujishima, Y.; Taguchi, Y.; Okada, Y.; Tokura, Y. *Physica B* **1993**, *188*, 1030.

10.1021/cm800934e CCC: $40.75
Published on Web 07/22/2008

Table 1. Synthesis Conditions, Phase Compositions, and Oxygen Nonstoichiometry of $Y_{1-x}Cd_xVO_{3+\delta}$

x	synthesis conditions[a]	impurities (mass fraction)	δ
0.5	1273 K, 1 h, Au	hp-YVO_4 (3%)	0.07
0.5	1273 K, 1 h, BN	no detectable impurities	0.07
0.4	1433 K, 1.5 h, Au	hp-YVO_4 (3%)	0.02
0.4	1433 K, 1 h, BN	Cd (0.5%)	0.02
1/3	1473 K, 1 h, BN	Cd (1%)	0.04
0.3	1433 K, 1.5 h, Au	an unknown delafossite-type phase (10%)[b]	*c*
0.3	1473 K, 1 h, BN	Cd (1%)	0.02

[a] Synthesis temperature, time, and a material surrounding the sample. All the syntheses were done at 6 GPa. [b] Space group *R*-3*m*, a = 3.5419(8) Å and c = 17.345(6) Å. Note that the similar impurity phase (phase I in ref 20) was found in samples with nominal compositions of $Cd_{0.9}VO_3$ and $CdVO_{3.1}$,[20] suggesting that this phase does not contain Y. [c] Not determined because of the large amount of impurity.

in $CaVO_3$. An IM transition was reported to occur near x = 0.6,[19] 0.5,[2,15] 0.4,[8] or 0.3.[17]

The high-pressure modification of $CdVO_3$ was reported to have the $GdFeO_3$-type perovksite structure (a = 5.33435 Å, b = 7.52320 Å, and c = 5.26394 Å), and it is metallic.[20] We recently investigated solid solutions $Y_{1-x}Cd_xVO_3$ prepared at a high pressure of 6 GPa and found[21] that (1) phase separation into two $GdFeO_3$-type phases takes place for $0.6 < x < 1$ in contrast to the $Y_{1-x}Ca_xVO_3$ system, where continuous solid solutions are reported,[15,17] (2) the IM transition occurs between x = 0.5 and 0.4 similar to the $Y_{1-x}Ca_xVO_3$ system,[2,15] and (3) in the vicinity of the IM transition (that is, in $Y_{0.6}Cd_{0.4}VO_3$) a new phase transition takes place near 150 K which has never been detected in the $Y_{1-x}Ca_xVO_3$ system[2] and whose origin has not been clarified.

In this work, we investigated the structural properties of $Y_{0.6}Cd_{0.4}VO_3$ using electron diffraction, laboratory, and synchrotron X-ray powder diffraction data. We found structural anomalies in a wide temperature range below 200 K in agreement with anomalies of physical properties. The structural data suggested that orbital correlations/fluctuations should play an important role in this phase transition.

2. Experimental Section

$Y_{0.6}Cd_{0.4}VO_3$ was prepared from a stoichiometric mixture of Y_2O_3, V_2O_3, V_2O_5, and CdO. The mixture was placed directly in an Au capsule or in a BN crucible (the BN crucible was placed into an Au capsule) and treated at 6 GPa in a belt-type high-pressure apparatus at 1433 K for 60−90 min (heating rate 130 K/min). After heat treatment, the samples were quenched to room temperature (RT) and the pressure was slowly released. The resultant samples were black dense pellets. X-ray powder diffraction (XRD) data of $Y_{0.6}Cd_{0.4}VO_3$ showed that the sample prepared in the Au capsule contained a small amount (3 mass %) of the high-pressure modification of YVO_4 (scheelite-type, space group $I4_1/a$) as an impurity, and the sample prepared in the BN crucible contained a small amount of metal Cd (see Table 1). We also prepared the $Y_{1-x}Cd_xVO_3$ samples with x = 0.5, 1/3, and 0.3 (see Table 1). We note that the larger the Y content, higher synthesis temperatures were required for preparation of samples. Throughout the paper the samples with the same x will be distinguished by the material surrounding the sample during the synthesis, for example, $Y_{0.6}Cd_{0.4}VO_3$(Au) and $Y_{0.6}Cd_{0.4}VO_3$(BN).

The oxygen content in the final products was determined by thermogravimetric analysis (δ in $Y_{1-x}Cd_xVO_{3+\delta}$). Samples were heated in air on a SII Exstar 6000 (TG-DTA 6200) system between 300 and 1100 K at a heating−cooling rate of 10 K/min in Pt holders. All samples showed a weight gain from 720−770 K reaching saturation above 970−1070 K. The oxygen content calculated from the total weight gain is given in Table 1. Because the δ values are rather small, the compositions are written as $Y_{1-x}Cd_xVO_3$ throughout the paper. The oxygen nonstoichiometry (when it was investigated) was detected in many solid solution systems, e.g., $Y_{1-x}Ca_xVO_{3+\delta}$ ($-0.1 \le \delta \le 0.03$ or $-0.06 \le \delta \le -0.01$)[15,17] and $La_{1-x}Sr_xVO_{3+\delta}$ ($0.01 \le \delta \le 0.05$).[22]

Here we would like to emphasize advantages of high-pressure synthesis in sealed capsules for preparation of $Y_{1-x}Cd_xVO_3$. First, this method prevents evaporation of Cd. Synthesis of $Y_{1-x}Ca_xVO_3$ requires annealing at high temperatures (1473 K) in a floating-zone furnace or in a reducing atmosphere. In the case of $Y_{1-x}Cd_xVO_3$, it will cause formation and evaporation of Cd. Synthesis in sealed quartz tubes is also problematic because of the high annealing temperatures and high vapor pressure of Cd. Second, in sealed capsules the total oxygen content is not changed. The small oxygen overstoichiometry in $Y_{1-x}Cd_xVO_3$ and formation of YVO_4 with V^{5+} as an impurity in bulk can be explained by reaction of CdO with Au on the surface.[20] When there was no contact between the samples and Au (that is, we used BN) and the synthesis temperature was high, self-reduction of CdO took place in bulk with formation of metallic Cd as an impurity and releasing oxygen. Third, because the perovskite $CdVO_3$ can be prepared only at high pressure, preparation of Cd-rich samples at ambient pressure may be impossible. Fourth, the high-pressure method directly gives dense pellets suitable for different measurements.

XRD data of $Y_{0.6}Cd_{0.4}VO_3$(Au) were collected with a RIGAKU RINT 2500 diffractometer (2θ range of 4−82°, a step width of 0.02°, and a counting time of 1 s/step) from 12 to 290 K. Synchrotron XRD data of $Y_{0.6}Cd_{0.4}VO_3$(Au) for the structure refinement were measured between 100 and 300 K on a large Debye−Scherrer camera at the BL02B2 beam line of SPring-8.[23] Incident beams from a bending magnet were monochromatized to λ = 0.77654 Å. The sample was contained in a glass capillary tube with an inner diameter of 0.1 mm and rotated during measurements. The synchrotron XRD data were collected in a 2θ range from 1° to 75° with a step interval of 0.01°. Structure parameters of YVO_3[6,10] were used as initial ones in the Rietveld refinement of $Y_{0.6}Cd_{0.4}VO_3$ at 300 K using RIETAN-2000 software.[24] At lower temperatures, the structure parameters obtained at the higher temperature were used as the initial ones. Coefficients for analytical approximation to atomic scattering factors for Y, Cd, V, and O were taken from ref 25. The pseudo-Voigt function of Toraya was used as a profile function.[26] The background was represented by an 11th-order Legendre polynomial. The occupancy factor, g, of all the sites was unity (g = 1). Isotropic atomic displacement parameters, B, with the isotropic Debye−Waller factor represented as $\exp((-B \sin^2\theta)/\lambda^2)$ were assigned to all the sites. For the

(20) Belik, A. A.; Takayama-Muromachi, E. *J. Solid State Chem.* **2006**, *179*, 1650.
(21) Belik, A. A.; Shpanchenko, R. V.; Takayama-Muromachi, E. *J. Magn. Magn. Mater.* **2007**, *310*, e240.
(22) Miyasaka, M.; Okuda, T.; Tokura, Y. *Phys. Rev. Lett.* **2000**, *85*, 5388.
(23) Nishibori, E.; Takata, M.; Kato, K.; Sakata, M.; Kubota, Y.; Aoyagi, S.; Kuroiwa, Y.; Yamakata, M.; Ikeda, N. *Nucl. Instrum. Methods Phys. Res., Sect. A* **2001**, *467−468*, 1045.
(24) Izumi, F.; Ikeda, T. *Mater. Sci. Forum* **2000**, *321−324*, 198.
(25) *International Tables for Crystallography*, 2nd ed.; Wilson, A. J. C., Prince, E., Eds.; Kluwer: Dordrecht, The Netherlands, 1999; Vol. I, pp 572−574.
(26) Toraya, H. *J. Appl. Crystallogr.* **1990**, *23*, 485.

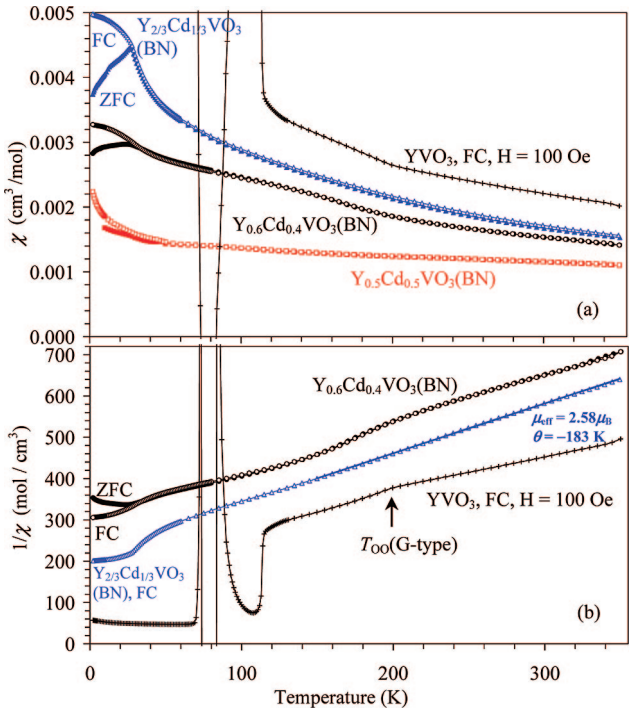

Figure 1. (a) ZFC (filled symbols) and FC (white symbols) χ vs T curves of the powder $Y_{0.5}Cd_{0.5}VO_3$(BN), $Y_{0.6}Cd_{0.4}VO_3$(BN), and $Y_{2/3}Cd_{1/3}VO_3$(BN) samples measured at 1000 Oe. The FC χ vs T curves of the powder YVO_3 sample (treated at 6 GPa and 1473 K) measured at 100 Oe are also given. Note the magnetization reversal in powder YVO_3 that has been observed for the first time. (b) The ZFC (filled symbols) and FC (white symbols) χ^{-1} vs T curves of the powder $Y_{0.6}Cd_{0.4}VO_3$(BN) sample, and FC χ^{-1} vs T curves of the powder $Y_{2/3}Cd_{1/3}VO_3$(BN) and YVO_3 samples. The solid line gives the Curie−Weiss fit for $Y_{2/3}Cd_{1/3}VO_3$(BN); the parameters (μ_{eff} and θ) of fitting are shown on the figure.

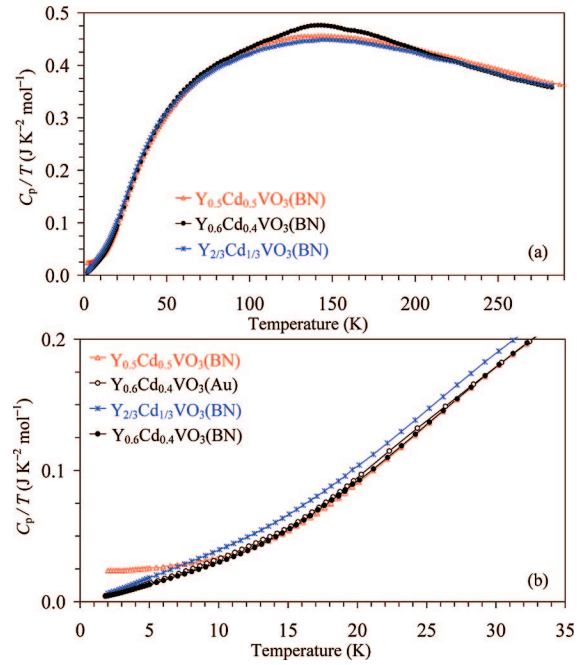

Figure 2. (a) C_p/T vs T curves of insulating $Y_{0.6}Cd_{0.4}VO_3$(BN) and $Y_{2/3}Cd_{1/3}VO_3$(BN) and metallic $Y_{0.5}Cd_{0.5}VO_3$(BN) between 2 and 300 K. (b) Low-temperature part of the C_p/T vs T curves of $Y_{0.6}Cd_{0.4}VO_3$(Au),[21] $Y_{0.6}Cd_{0.4}VO_3$(BN), $Y_{2/3}Cd_{1/3}VO_3$(BN), and $Y_{0.5}Cd_{0.5}VO_3$(BN).

impurity of YVO_4 we refined only a scale factor and the lattice parameters, fixing its structure parameters.[27] The mass percentage of YVO_4 in $Y_{0.6}Cd_{0.4}VO_3$(Au) was calculated from the refined scale factors.

Direct current (dc) magnetic susceptibilities (χ = **M/H**) were measured on a Quantum Design SQUID magnetometer (MPMS) between 2 and 400 K in an applied field of 1000 Oe under both zero-field-cooled (ZFC) and field-cooled (FC) conditions. Specific heat, C_p, was recorded between 2 and 300 K on cooling at zero magnetic field by a pulse relaxation method using a commercial calorimeter (Quantum Design PPMS). Electrical resistivity was measured between 2 and 300 K by the conventional four-probe method using a Quantum Design PPMS with the ac-gage current of 1 mA at 30 Hz.

For selected-area electron diffraction (SAED) studies the $Y_{0.6}Cd_{0.4}VO_3$(Au) sample was crushed under CCl_4 and then dispersed on a Cu grids coated with a carbon film for transmission electron microscopy. The SEAD experiments were carried out using a Hitachi HF-3000S operated at 300 kV between 80 and 300 K.

3. Results and Discussion

3.1. Physical Properties of $Y_{1-x}Cd_xVO_3$. Figure 1 shows the ZFC and FC magnetic susceptibilities of $Y_{0.6}Cd_{0.4}VO_3$(BN). Very similar curves were observed in $Y_{0.6}Cd_{0.4}VO_3$(Au) (see the Supporting Information).[21] Both samples demonstrated the same features: (1) the difference between the ZFC and FC curves below 35 K and (2) change in the slope of the χ^{-1} vs T curve in a wide temperature range between 130 and 200 K. We investigated the properties of $Y_{1-x}Cd_xVO_3$ with x = 0.5, 1/3, and 0.3 to see whether this behavior is retained or not. There was a sharp anomaly at 28 K on the ZFC magnetic susceptibility curve of $Y_{2/3}Cd_{1/3}VO_3$(BN) and a sudden drop of the inverse magnetic susceptibility below 50 K. The difference between the ZFC and FC curves is observed below 28 K. However, there was no slope change on the χ^{-1} vs T curve above 50 K (Figure 1b). $Y_{0.5}Cd_{0.5}VO_3$(BN) and $Y_{0.5}Cd_{0.5}VO_3$(Au)[21] showed almost temperature-independent paramagnetism in agreement with their metallic state (Figure 1 and the Supporting Information).

Specific heat measurements clearly showed a very broad anomaly between 110 and 180 K in $Y_{0.6}Cd_{0.4}VO_3$ in comparison with $Y_{0.5}Cd_{0.5}VO_3$ and $Y_{2/3}Cd_{1/3}VO_3$ (Figure 2) where no anomalies were found at all. The C_p/T vs T curves of $Y_{0.6}Cd_{0.4}VO_3$ and $Y_{2/3}Cd_{1/3}VO_3$ went to the origin in agreement with their insulating state. On the other hand, specific heat measurements of $Y_{0.5}Cd_{0.5}VO_3$ clearly showed the electronic contribution at low temperatures in agreement with its metallic state. Note that the specific heat data were the same for $Y_{0.6}Cd_{0.4}VO_3$(BN) and $Y_{0.6}Cd_{0.4}VO_3$(Au) (see Figure 2b for the low-temperature part and the Supporting Information for the whole data). This fact (coupled with the very similar magnetic susceptibility curves) shows that small variations in the stoichiometry of $Y_{0.6}Cd_{0.4}VO_3$(BN) and $Y_{0.6}Cd_{0.4}VO_3$(Au) that should take place because of the presence of different impurities have almost no effect on their physical properties. EDX analysis also gave the same cation composition for $Y_{0.6}Cd_{0.4}VO_3$(BN) and $Y_{0.6}Cd_{0.4}VO_3$(Au) within experimental error. On the other hand, the specific heat of $Y_{0.5}Cd_{0.5}VO_3$(BN) and $Y_{0.5}Cd_{0.5}VO_3$(Au) at the lowest

(27) Wang, X.; Loa, I.; Syassen, K.; Hanfland, M.; Ferrand, B. *Phys. Rev. B* **2004**, *70*, 064109.

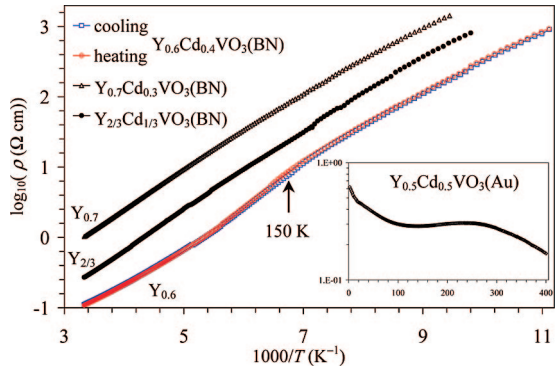

Figure 3. Resistivity curves of insulating $Y_{0.6}Cd_{0.4}VO_3$(BN), $Y_{2/3}Cd_{1/3}VO_3$(BN), and $Y_{0.7}Cd_{0.3}VO_3$(BN) plotted as $\log_{10}\rho$ vs $10^3/T$. (Inset) Resistivity curve of $Y_{0.5}Cd_{0.5}VO_3$(Au).[21]

temperatures was slightly different (see the Supporting Information), indicating that the metallic state near the IM transition was affected by small variations in stoichiometry.

No anomalies were found on specific heat curves near 35 K in $Y_{0.6}Cd_{0.4}VO_3$ and 28 K in $Y_{2/3}Cd_{1/3}VO_3$. Therefore, the difference between the ZFC and FC curves could arise from a spin-glass transition. However, ac susceptibility studies showed no frequency dependence for $Y_{0.6}Cd_{0.4}VO_3$ and $Y_{2/3}Cd_{1/3}VO_3$ (see the Supporting Information). In addition, almost the same difference between ZFC and FC curves was observed at 50 kOe (see the Supporting Information). For a spin-glass (and also for contributions from impurities), a high magnetic field should eliminate the difference between the ZFC and FC curves. Because of the presence of magnetic ions (V^{3+} and V^{4+}) in corner-shared octahedra some magnetic interactions/correlations should take place. However, sometimes specific heat anomalies at the onset of long-range magnetic ordering are completely suppressed due to strong frustration (e.g., two-dimensional systems)[28] or a small ordered magnetic moment. In $Y_{0.6}Cd_{0.4}VO_3$ and $Y_{2/3}Cd_{1/3}VO_3$ there is a random distribution of V^{3+} and V^{4+} ions at one crystallographic site. This disordering can also suppress specific heat anomalies. Therefore, we can assume that long-range magnetic ordering takes place in $Y_{0.6}Cd_{0.4}VO_3$ and $Y_{2/3}Cd_{1/3}VO_3$ below 35 and 28 K, respectively. However, this assumption needs further confirmation, for example, using muon spin relaxation measurements.

The resistivity measurements of the insulating phases $Y_{0.6}Cd_{0.4}VO_3$, $Y_{2/3}Cd_{1/3}VO_3$, and $Y_{0.7}Cd_{0.3}VO_3$ confirmed the existence of the anomaly near 150 K in $Y_{0.6}Cd_{0.4}VO_3$ in comparison with $Y_{2/3}Cd_{1/3}VO_3$ and $Y_{0.7}Cd_{0.3}VO_3$ (Figure 3). Therefore, measurements of the physical properties indicated the unique properties of $Y_{0.6}Cd_{0.4}VO_3$. The phase transition found in $Y_{0.6}Cd_{0.4}VO_3$ has never been detected in the $Y_{1-x}Ca_xVO_3$system.[2]Confirming the unique physical properties of $Y_{0.6}Cd_{0.4}VO_3$, we moved to the investigation of its structural properties to understand the origin of this anomalous behavior. Here we note that only nonmagnetic impurities (YVO_4 and Cd) were found in $Y_{1-x}Cd_xVO_3$ with $x = 0.3$, 1/3, 0.4, and 0.5 (except for $Y_{0.7}Cd_{0.3}VO_3$(Au), where an unknown delafossite-type phase gives a strong ferromagnetic response below 70 K). Therefore, these impurities should have no effect on the measured physical properties.

3.2. Structural Properties of $Y_{0.6}Cd_{0.4}VO_3$. $Y_{0.6}Cd_{0.4}VO_3$ was found to crystallize in the $GdFeO_3$-type perovskite structure at 300 K (space group *Pnma*) similar to YVO_3.[6,10] Careful analysis of the high-resolution synchrotron XRD data of $Y_{0.6}Cd_{0.4}VO_3$ revealed that the *Pnma* structure was stable between 100 and 300 K. That is, neither additional reflections nor reflection splitting were detected. Note that the monoclinic distortion of YVO_3 observed between 77 and 200 K is extremely small, and single crystals and high-intensity synchrotron data were required to detect the *Pnma*−$P2_1/a$ phase transition.[5,10] Attempts to refine the crystal structure of $Y_{0.6}Cd_{0.4}VO_3$ in space group $P2_1/a$ at 100 and 300 K gave no noticeable improvement of the fitting. No evidence for the symmetry change of $Y_{0.6}Cd_{0.4}VO_3$ was also found in the laboratory XRD data down to 12 K. The lattice parameters between 20 and 280 K were refined, adopting the *Pnma* model using RIETAN-2000.[24]

Electron diffraction observations between 80 and 300 K also confirmed that the crystal symmetry of $Y_{0.6}Cd_{0.4}VO_3$ does not change through the phase transition (Figure 4). Therefore, these results rule out the possibility of extremely small structural distortion and symmetry lowering (for example, due to tiny rotation of oxygen octahedra). Note that some forbidden spots observed in Figure 4 are due to the double diffraction.

Figure 5 shows the temperature dependence of lattice parameters between 20 and 280 K. Clear anomalies were observed between 120 and 180 K where a broad anomaly on the specific heat and change of the slope of the inverse magnetic susceptibility were found (Figures 1 and 2). The *c* parameter linearly decreased from 20 to 120 K, and then it lineally increased from 160 to 300 K. The *b* parameter was constant between 20 and 120 K, demonstrated a rather sudden drop from 120 to 200 K, and then lineally increased from 200 to 300 K. The *a* parameter increased monotonically with temperature with a small bump near 180 K. The unit cell volume also showed an anomalous gradual decrease with temperature from 120 to 180 K.

Final lattice parameters, *R* factors, fractional coordinates, *B* parameters, and some bond lengths of $Y_{0.6}Cd_{0.4}VO_3$(Au) at selected temperatures are listed in Table 2. Figure 6 displays observed, calculated, and difference synchrotron XRD patterns of $Y_{0.6}Cd_{0.4}VO_3$(Au) at 300 K as an example. Figure 7b shows the temperature dependence of the V−O bond lengths. Between 150 and 300 K there were very small changes in the V−O bond lengths. The V−O2 bond lengths were the same within standard deviations (1.972 and 1.976 Å at 300 K). Below 150 K, the V−O2 distances lying in the ac plane (Figure 8) started to split into two short V−O2 distances (1.961 Å at 100 K) and two long V−O2 distances (1.983 Å at 100 K). This splitting was not as large as, for example, in YVO_3 (1.99 and 2.05 Å) during the *G*-type orbital ordering transition below 200 K. We note that the splitting slightly reduces in the *C*-type orbital-ordered state of YVO_3 below 77 K (1.99 and 2.04 Å).[5,6,10] However, the

(28) Lancaster, T.; Blundell, S. J.; Brooks, M. L.; Baker, P. J.; Pratt, F. L.; Manson, J. L.; Conner, M. M.; Xiao, F.; Landee, C. P.; Chaves, F. A.; Soriano, S.; Novak, M. A.; Papageorgiou, T. P.; Bianchi, A. D.; Herrmannsdoerfer, T.; Wosnitza, J.; Schlueter, J. A. *Phys. Rev. B* **2007**, *75*, 094421.

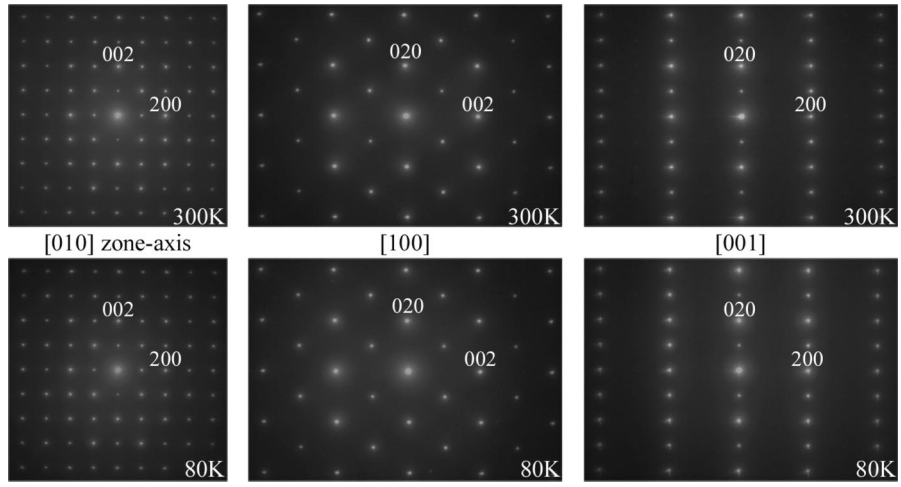

Figure 4. Selected-area electron diffraction patterns of $Y_{0.6}Cd_{0.4}VO_3$(Au) at 300 and 80 K.

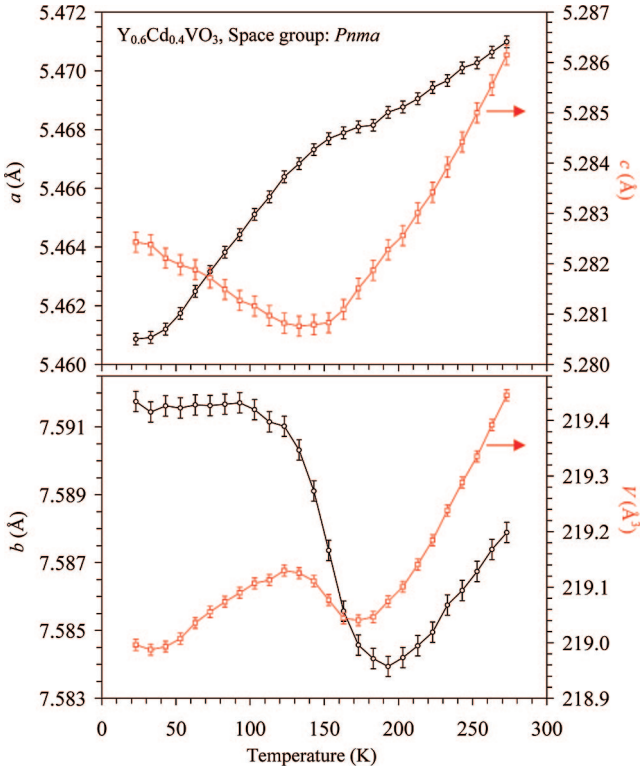

Figure 5. Temperature dependence of the lattice parameters (*a*, *b*, and *c*) and unit cell volume (*V*) in $Y_{0.6}Cd_{0.4}VO_3$(Au) between 20 and 280 K.

tendency for the splitting of V−O2 distances in $Y_{0.6}Cd_{0.4}VO_3$ was very clear. Unfortunately the high-quality data for the structure refinement were not available below 100 K to track the evolution of the V−O bond lengths at lower temperatures.

In ref 29 it was suggested that the lattice parameter ratio *a*/*c* (*b*/*a* in *Pbnm*) may serve as an indicator of the type of orbital ordering. For example, the appearance of the *C*-type orbital order in YVO_3, $HoVO_3$, and $YbVO_3$ is accompanied by a large drop of the *a*/*c* ratio. Figure 7a shows the temperature dependence of the lattice parameter ratios ($\sqrt{2}a/b$, $b/\sqrt{2}c$, and *a*/*c*) in $Y_{0.6}Cd_{0.4}VO_3$. The rather sharp maximum was observed on the *a*/*c* vs *T* curve of $Y_{0.6}Cd_{0.4}VO_3$. However, the transition is continuous similar to $SmVO_3$ and in contrast to discontinuous first-order transitions in YVO_3, $HoVO_3$, and $YbVO_3$.[29] Therefore, the temperature dependence of the V−O distances and the *a*/*c* ratio in $Y_{0.6}Cd_{0.4}VO_3$ gives support that orbital correlations play an important role in the observed phase transition near 150 K.

Anomalies of physical properties at the orbital order and spin order transitions in the undoped samples (YVO_3 and so on) are rather sharp. There is a slope change of magnetic susceptibilities during the *G*-type orbital order in YVO_3 (Figure 1). Because spin orders take place below 116 and 77 K, it is impossible to see the effect of the *C*-type orbital order on magnetic susceptibilities of YVO_3. The crystal symmetry of YVO_3 is *Pnma* above 200 K and $P2_1/a$ in the *G*-type orbital-ordered state. The crystal symmetry is restored (*Pnma*) in the *C*-type orbital-ordered state.

In $Y_{0.6}Cd_{0.4}VO_3$ the phase transition near 150 K takes place in a wide temperature range, and inverse magnetic susceptibilities change their slope. Electron diffraction unambiguously confirmed that the crystal symmetry is retained between 80 and 300 K. All these facts do not contradict with the *C*-type orbital correlations. The occurrence of the phase transition in a wide temperature range can be explained by a random distribution of V^{3+} and V^{4+} ions (similar to the absence of specific heat anomaly at 35 K) and the fact that the V^{3+}:V^{4+} ratio is far from, say, 1:1 or 1:2. Therefore, the orbital correlations develop slowly on decreasing temperature.

For compositions with V^{3+}:V^{4+} ratio of 1:1 or 2:1, one could expect charge ordering transitions. However, no phase transitions were detected in $Y_{0.5}Cd_{0.5}VO_3$ and $Y_{2/3}Cd_{1/3}VO_3$ (Figures 1−3). This fact shows that charge-ordered states probably are not realized in the $Y_{1-x}Cd_xVO_3$ system. The $Y_{0.6}Cd_{0.4}VO_3$ composition is located near the IM boundary, and phase separation to metallic and insulating phases could take place at low temperatures. However, the specific heat (Figure 2: the absence of electronic contribution) and resistivity (Figure 3) measurements clearly showed the absence of a metallic phase at low temperatures in $Y_{0.6}Cd_{0.4}VO_3$. In addition, electron diffraction data at 80 K

(29) Sage, M. H.; Blake, G. R.; Nieuwenhuys, G. J.; Palstra, T. T. M. *Phys. Rev. Lett.* **2006**, *96*, 036401.

Table 2. Structural Parameters, *R* Factors (%), and Bond Lengths (Å) of $Y_{0.6}Cd_{0.4}VO_3$ at Selected Temperatures As Determined from Rietveld Refinements Based on the Synchrotron X-Ray Powder Diffraction Data[a]

	T (K)					
	100	130	150	170	200	300
a (Å)	5.44872(3)	5.45125(2)	5.45245(2)	5.45239(2)	5.45257(2)	5.45887(3)
b (Å)	7.57074(4)	7.57070(4)	7.56813(3)	7.56423(3)	7.56268(3)	7.57250(4)
c (Å)	5.26806(3)	5.26802(2)	5.26764(2)	5.26724(2)	5.26784(2)	5.27643(2)
x (Y/Cd)	0.05250(8)	0.05257(7)	0.05258(7)	0.05249(7)	0.05237(7)	0.05202(6)
$-z$ (Y/Cd)	0.01113(13)	0.01134(12)	0.01137(11)	0.01156(11)	0.01154(11)	0.01132(10)
B (Y/Cd)	0.363(11)	0.357(10)	0.370(9)	0.358(9)	0.423(9)	0.569(9)
B (V)	0.177(16)	0.172(15)	0.184(13)	0.172(13)	0.212(13)	0.273(13)
x (O1)	0.4657(7)	0.4654(6)	0.4660(6)	0.4665(5)	0.4671(5)	0.4671(5)
z (O1)	0.0956(7)	0.0953(6)	0.0956(6)	0.0947(5)	0.0943(5)	0.0956(5)
B (O1)	0.20(7)	0.25(7)	0.29(6)	0.29(6)	0.32(6)	0.45(6)
x (O2)	0.2980(5)	0.2983(5)	0.2989(4)	0.2988(4)	0.2986(4)	0.2994(4)
y (O2)	0.0508(4)	0.0504(4)	0.0501(3)	0.0502(3)	0.0502(3)	0.0497(3)
z (O2)	0.6956(5)	0.6959(5)	0.6965(4)	0.6967(4)	0.6969(4)	0.6966(4)
B (O2)	0.35(6)	0.32(5)	0.28(5)	0.30(4)	0.35(4)	0.41(4)
R_{wp}	6.64	6.25	5.76	5.61	5.62	5.41
R_p	4.66	4.49	4.23	4.04	4.02	4.02
R_B	2.10	2.06	1.78	1.85	1.82	2.12
R_F	1.20	1.13	0.96	0.92	0.96	1.14
S	3.59	3.28	2.99	2.87	2.81	2.56
V−O1 × 2	1.967(1)	1.967(1)	1.966(1)	1.964(1)	1.963(1)	1.967(1)
V−O2 × 2	1.961(3)	1.964(3)	1.967(2)	1.968(2)	1.967(2)	1.972(2)
V−O2 × 2	1.983(3)	1.980(3)	1.975(2)	1.975(2)	1.975(2)	1.976(2)

[a] Space group *Pnma* (No 62). (0.6Y/0.4Cd), V, O1, and O2 atoms occupy the $4c(x,1/4,z)$, $4b(0,0,1/2)$, $4c(x,1/4,z)$, and $8d(x,y,z)$ sites, respectively. The unit of *B* is $Å^2$. Numbers in parentheses are statistical errors of the last significant digits.

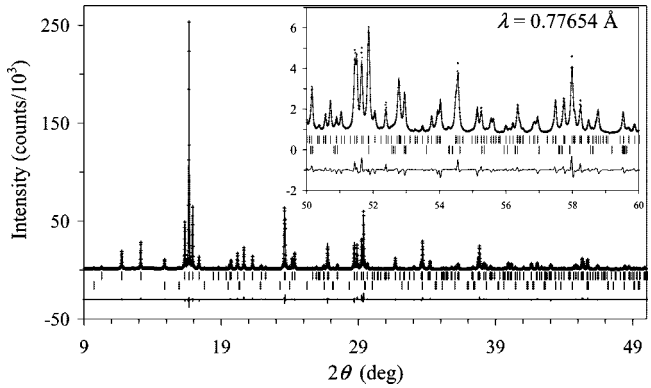

Figure 6. Observed (crosses), calculated (solid line), and difference patterns resulting from Rietveld analysis of the synchrotron X-ray powder diffraction data of $Y_{0.6}Cd_{0.4}VO_3$(Au) at room temperature. Bragg reflections are indicated by tick marks. The lower tick marks are given for reflections from the impurity hp-YVO_4 (3 mass %).

and high-resolution synchrotron XRD data at 100 K gave no evidence for phase separation.

It is known that the *G*- and *C*-type orbital orders of YVO_3 are drastically suppressed by substitution in the $Y_{1-x}Ca_xVO_3$ system. For example, the *C*-type orbital order disappears around $x = 0.02$, and the *G*-type orbital order disappears at $x > 0.1$.[2] No anomalies were found on specific heat of $Y_{1-x}Ca_xVO_3$ for $x > 0.11$.[2] To the best of our knowledge, at higher doping concentrations no phase transitions involving orbital/charge degrees of freedom are reported in the $Y_{1-x}Ca_xVO_3$ and $Y_{1-x}Sr_xVO_3$ systems. In the $Y_{1-x}Cd_xVO_3$ system, $Y_{0.6}Cd_{0.4}VO_3$ ($x = 0.4$) lying near the IM boundary is a unique composition because other samples (e.g., $x = 0.3$, 1/3, and 0.5) did not show similar phase transitions. The absence of a phase transition in $Y_{0.5}Cd_{0.5}VO_3$ may be explained by the fact that this compound shows metallic properties. Therefore, we can assume that a new type of phase transition for MVO_3 involving orbital correlations takes place in the highly doped $Y_{0.6}Cd_{0.4}VO_3$. In e_g orbitally

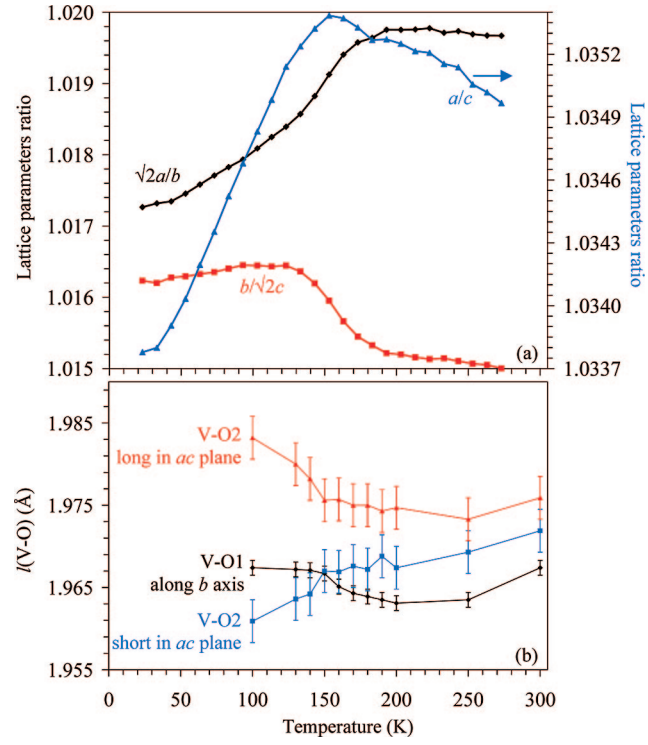

Figure 7. (a) Temperature dependence of the ratios between the lattice parameters ($\sqrt{2}a/b$, $b/\sqrt{2}c$, and a/c) in $Y_{0.6}Cd_{0.4}VO_3$(Au) between 20 and 280 K. (b) Temperature dependence of the V−O bond lengths in $Y_{0.6}Cd_{0.4}VO_3$(Au) between 100 and 300 K.

ordered systems such as $MMnO_3$ (M = La, Pr, and Bi) different orbital orders exist in lightly and highly doped samples, for example, in $Bi_{0.75}Sr_{0.25}MnO_3$, $Bi_{0.31}Ca_{0.69}MnO_3$,[30–32] and $Pr_{0.6}Ca_{0.4}MnO_3$.[33]

In conclusion, the structural properties of $Y_{0.6}Cd_{0.4}VO_3$ were investigated. The phase transition near 150 K has the intrinsic nature. No symmetry change was found through this phase transition. It is accompanied by significant anomalies in the temperature dependence of the lattice parameters and

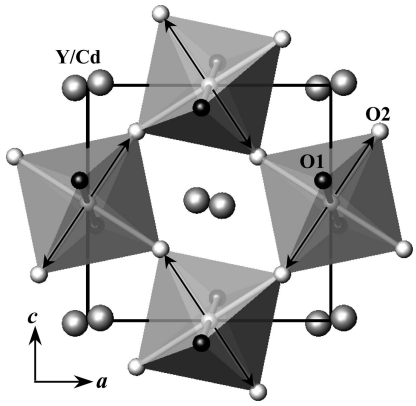

Figure 8. Projections of the crystal structure of $Y_{0.6}Cd_{0.4}VO_3$ along the *b* axis. The V−O2 bond lengths elongated below 150 K are marked with the arrows.

ratios between the lattice parameter. The V−O bond lengths are split to shorter and longer ones, indicating that orbital correlations play an important role in this phase transition. We hope that our findings will stimulate more detailed investigations of doped vanadates $R_{1-x}M_xVO_3$ (R = Y and rare earths and M = Ca, Sr, and Cd).

Acknowledgment. This work was supported by the World Premier International Research Center Initiative (WPI Initiative, MEXT, Japan) and a NIMS Individual-Type Competitive Research Grant. The synchrotron radiation experiments were performed at the SPring-8 with the approval of the Japan Synchrotron Radiation Research Institute.

Supporting Information Available: ac susceptibility curves for $Y_{0.6}Cd_{0.4}VO_3$(Au) and $Y_{2/3}Cd_{1/3}VO_3$(BN) (Figure S1); dc susceptibility curves for $Y_{0.6}Cd_{0.4}VO_3$(Au) measured at 1 and 50 kOe (Figure S2); TG curves of $Y_{0.6}Cd_{0.4}VO_3$(Au) and $Y_{0.6}Cd_{0.4}VO_3$(BN) (Figure S3); comparison of magnetic susceptibilities and specific heat for different samples (Figures S4−S7) (PDF). This material is available free of charge via the Internet at http://pubs.acs.org.

CM800934E

(30) Goff, R. J.; Attfield, J. P. *J. Solid State Chem.* **2006**, *179*, 1369.
(31) Grenier, S.; Kiryukhin, V.; Cheong, S. W.; Kim, B. G.; Hill, J. P.; Thomas, K. J.; Tonnerre, J. M.; Joly, Y.; Staub, U.; Scagnoli, V. *Phys. Rev. B* **2007**, *75*, 085101.
(32) Pissas, M.; Margiolaki, I.; Papavassiliou, G.; Stamopoulos, D.; Argyriou, D. *Phys. Rev. B* **2005**, *72*, 064425.
(33) von Zimmermann, M.; Hill, J. P.; Gibbs, D.; Blume, M.; Casa, D.; Keimer, B.; Murakami, Y.; Tomioka, Y.; Tokura, Y. *Phys. Rev. Lett.* **1999**, *83*, 4872.